Desalination 537 (2022) 115898

Contents lists available at ScienceDirect

Desalination

journal homepage: www.elsevier.com/locate/desal

Immobilized graphene oxide-based membranes for improved pore wetting resistance in membrane distillation

Monica Alberto [a,1], Clara Skuse [a], Marzieh Tamaddondar [b], Patricia Gorgojo [a,c,d,*]

[a] Department of Chemical Engineering, Faculty of Science and Engineering, The University of Manchester, Manchester M13 9PL, United Kingdom
[b] Department of Materials, The University of Manchester, Oxford Road, Manchester M13 9PL, United Kingdom
[c] Nanoscience and Materials Institute of Aragón (INMA) CSIC-Universidad de Zaragoza, C/Mariano Esquillor s/n, 50018 Zaragoza, Spain
[d] Chemical and Environmental Engineering Department, Universidad de Zaragoza, C/Pedro Cerbuna 12, 50009 Zaragoza, Spain

HIGHLIGHTS

- GO laminate membranes were synthesized onto commercial porous PVDF substrates.
- Immobilization was achieved using polydopamine as an anchor molecule.
- Permeate flux was not affected by additional layers.
- Membranes were stable for over 90 h with feed solutions containing surfactants.

GRAPHICAL ABSTRACT

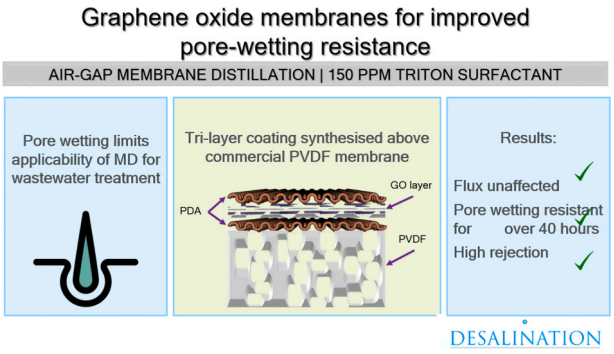

ARTICLE INFO

Keywords:
Graphene oxide (GO)
Membrane distillation (MD)
Pore wetting resistance
Surfactant
Wastewater treatment

ABSTRACT

Membrane distillation (MD) is a useful method for the purification of difficult feedwaters but it cannot be applied in a range of industries due to pore wetting. In this work, graphene oxide (GO) laminate coatings are explored to overcome the pore wetting issues. Air gap MD (AGMD) configuration was considered, using a 35 g L^{-1} NaCl solution with 150 mg L^{-1} (150 ppm) of Triton X-100 surfactant as feed material. The GO is deposited as a laminate membrane on top of a commercial porous polyvinylidene fluoride (PVDF) support and good adhesion is achieved through the use of polydopamine (PDA) to form a hydrophilic tri-layer membrane. The small pore size achieved with the laminate GO led to increased pore wetting resistance for at least 90 h compared to 20 min with pristine commercial PVDF. Additionally, the extra layers of GO and PDA did not affect the membrane flux. Overall, a tri-layer immobilized GO membrane is synthesized with superior performance when compared to current commercial membranes, meaning that MD can be used for a new range of wastewater applications.

* Corresponding author at: Chemical and Environmental Engineering Department, Universidad de Zaragoza, C/ Pedro Cerbuna 12, 50009 Zaragoza, Spain.
E-mail address: pgorgojo@unizar.es (P. Gorgojo).
[1] Present address: Department of Materials, The University of Manchester, Oxford Road, Manchester M13 9PL, United Kingdom.

https://doi.org/10.1016/j.desal.2022.115898
Received 3 March 2022; Received in revised form 11 May 2022; Accepted 3 June 2022
Available online 11 June 2022

1. Introduction

Water scarcity is a global issue which is expected to reduce people's accessibility to potable water in the coming decades, with the UN reporting that 5 billion people will be living in water scarce areas for at least one month by 2050 [1]. As a solution, the production of clean drinking water from non-conventional water/wastewater sources needs to be explored. Membrane distillation (MD) is a promising separation method for water and wastewater treatment, addressing the increasingly stringent water quality standards and environmental regulations. MD is a thermally driven separation process that employs a hydrophobic porous membrane (e.g. polypropylene (PP) [2], polytetrafluoroethylene (PTFE) [3], and polyvinylidene fluoride (PVDF) [4]). The hydrophobic nature of the membrane prevents the penetration of the liquid feed solution into its pores, allowing only the passage of water vapor driven by the partial water vapor pressure difference across the membrane (Fig. 1a) [5]. MD features several advantages compared to conventional separation processes including, but not limited to: operation at low pressures and temperatures (which leads to low operation cost and process safety), and low-grade energy use (e.g. solar thermal energy, waste heat) which makes MD a more cost-effective and environmentally friendly process. MD can also achieve higher water recoveries when compared to RO, this is because the energy consumption does not depend on the feed concentration [6,7]. This also means that MD can treat difficult, highly concentrated feedwaters that would be too energy intensive to be considered via RO [8]. Other conventional water treatment methods such as microfiltration (MF), ultrafiltration (UF) and nanofiltration (NF) have a lower specific energy consumption (SEC) but the membrane rejection is too low (70–85 %) to ensure the production of safe drinking water. As only volatile substances can cross the membrane in MD, the rejection is extremely high (>99 %) [9]. This would ensure complete removal of contaminants which cannot remain in the feed. Despite all the promising aspects of MD, pore wetting [6,10], and fouling [11] are aspects that limit the use of MD commercially.

Pore wetting refers to the penetration of the feed solution into the membrane pores and consequent process failure either by reducing the salt rejection or the permeate flux [12]. Pore wetting can be induced by the presence of low surface tension liquids that are miscible with water of the feed solution (e.g. alcohols [13]), and amphiphilic molecules (e.g. surfactants [6,13,14]). The understanding of the mechanisms behind the induction of pore wetting by these agents remains unclear, but fundamental insights have been developed in recent years. With this respect, Wang et al. suggested that pore wetting mechanisms induced by ethanol and Triton X-100 are different; alcohol-induced pore wetting occurs instantly whereas surfactant pore wetting is progressive and its kinetics depends on the vapor flux and the bulk concentration of surfactants in the feed solution [13]. The surfactants (which are amphiphilic molecules) adsorb onto the membrane surface and lower the liquid entry pressure (LEP). This impacts the gas-liquid interface and allows the feedwater to breach the membrane pores. After sufficient adsorption of surfactants, the LEP is reduced to the point where liquid water completely enters the pores and leads to the passage of feedwater through the membrane (Fig. 1b).

Several strategies have been reported to overcome this technical challenge. A review by Abdel-Karim et al. [15] evaluated cleaning regimes such as chemical treatment with citric acid and pre-treatment using foam fractionation to successfully remove foulants such as surfactants. However, cleaning can cause the deterioration of the membrane surface and a reduction in the contact angle, which leads to a reduction in pore-wetting resistance. The review concluded by suggesting that self-cleaning membranes need to be further developed and paired with appropriate cleaning strategies to better manage fouling and pore wetting in MD.

Self-cleaning membranes are highly resistant to pore wetting and fouling and have been explored as omniphobic membranes [16–19], superamphiphobic membranes [20], composite membranes with a hydrophilic coating [21,22], and combining material and operational approaches using a superhydrophobic membrane with air-layer recharging [23,24]. Similar to other challenges in membrane technology, graphene-based materials have been explored not only to tackle this issue but also to improve membrane performance such as improved rejection and higher permeate flux [5,25–27]. In this context, Seo et al. [28] transferred chemical vapor deposited (CVD) graphene onto PFTE and used it as an active layer for direct contact MD (DCMD) experiments. These membranes showed high water flux (~50 L m^{-2} h^{-1}), excellent NaCl rejection (99 %) when processing highly saline water and excellent antifouling properties. Moreover, Qiu et al. [27] modified the pore channel surface of PVDF membranes with graphene oxide (GO) for improved anti-fouling properties and distillate flux. Despite the promising results, the stability of laminated GO films onto hydrophobic porous membranes in aqueous media might be still an issue for MD applications. To prevent contamination of GO within the feedwater and to ensure robustness (i.e. membranes that are easy to handle), secure immobilization is required. Polydopamine (PDA) is a hydrophilic polymer with excellent binding properties to almost all substrates through the self-polymerization of dopamine under alkaline conditions [29–31]. It has been employed to enhance the compatibility, interfacial adhesion, and consequently stability of GO laminate membranes for pervaporation [31]. However, this is the first time PDA is being explored for the potential immobilization and mechanical protection of GO onto MD membranes for improved pore wetting and anti-fouling resistance.

The successful surface modification of commercial PVDF membranes to produce the PDA and GO layers is demonstrated in this study. For the first time, feed solutions with high concentrations (150 ppm) of

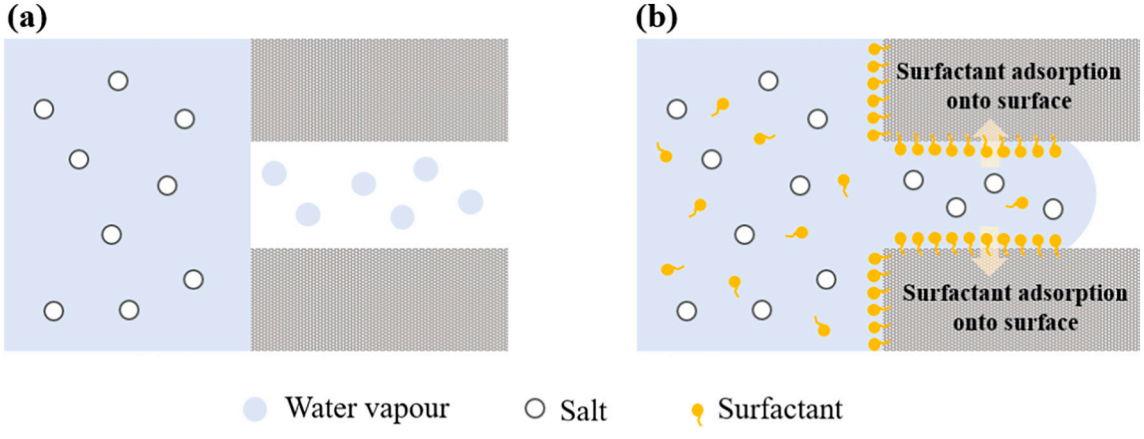

Fig. 1. (a) Non-wetted membrane, (b) pore-wetted membrane depicted by the presence of surfactants in the feedwater.

surfactants (Triton X-100) are treated with high rejections via MD. Desalination performance was evaluated in DCMD and air gap (AGMD) membrane distillation with feed solution containing low surface tension contaminants, including surfactants and mineral oil. Pore wetting and fouling were detected by monitoring the membrane flux and permeate conductivity.

2. Experimental section

2.1. Materials

Graphene oxide (GO) was purchased from William Blythe (UK). Dopamine hydrochloride (DA, 99 %), Tris(hydroxymethyl)aminomethane (Tris-HCl, pH = 8.5, 0.5 M), and Triton X-100 were purchased from Alfa Aesar (UK). Triton X-100 is a non-ionic surfactant with 100 % activity with a surface tension of 33 mN m^{-1} (1 % actives, 25 °C). It is representative of the type of surfactants which are used in paper-milling and textile processes. Isopropyl alcohol (IPA, ≥99.7 %) was purchased from WWR International (UK). PVDF membranes with a nominal pore size of 0.22 μm and average thickness of 125 μm (GVHP09050), ethanol (≥99.0 %), and sodium chloride (NaCl, ≥99.0 %) were purchased from Merck Life Science UK Limited (UK).

2.2. Membrane preparation

A doubled PDA coating was employed to enhance: (1) the compatibility between the hydrophobic commercial PVDF membrane and laminated GO membranes, and (2) the stabilization of GO membranes, preventing their potential delamination and leaching into the aqueous feed solutions, as well as providing mechanical stability. Thus, the preparation of the laminated GO membranes consists of three steps, as shown in Fig. 2: (1) modification of the PVDF membrane surface with a thin polydopamine (PDA) layer, (2) assembly of the bidimensional GO flakes by vacuum filtration of GO dispersion through the PDA-modified PVDF membranes, and (3) coating of the laminate GO membrane with a thin PDA layer.

Firstly, 2 mg mL^{-1} of DA was dissolved in a Tris-HCl buffer solution (pH = 8.5, 15 mM) and sonicated for 10 min. Commercial PVDF membranes were floated in that solution for 2 h, rinsed thoroughly with DI water and dried in a vacuum oven for 2 h at 60 °C. Subsequently, the modified PVDF membranes were immersed in IPA for 30 min to allow their full wetting and used for the deposition of GO through vacuum filtration. Different amounts of GO were dispersed in water/IPA with a volume ratio of water to IPA of 1:1, making up a concentration of 2 mg L^{-1}, and filtered through the IPA-impregnated PDA-modified membranes. These GO laminate membranes were dried at 60 °C for 2 h under vacuum. Finally, they were coated with a thin layer of PDA following the same procedure that was done to modify the surface of PVDF membranes. Pristine PVDF membranes coated with two 2 h-PDA coatings

Table 1
Membrane codes according to their composition. PDA coatings in steps 1 and 2 were performed with a 2 mg mL^{-1} DA in 10 mM Tris-HCl (pH 8.5) solution.

Membrane code	PDA coating time (h) (Step 1)	GO density (mg m^{-2}) (Step 2)	PDA coating time (h) (Step 3)
PVDF	–	–	–
2-PDA	2	–	–
2 + 2PDA	2 + 2	–	–
GO-PVDF	–	90.6	–
GO-PDA-PVDF	2	90.6	–
20GO	2	45.3	2
40GO	2	90.6	2
60GO	2	135.9	2

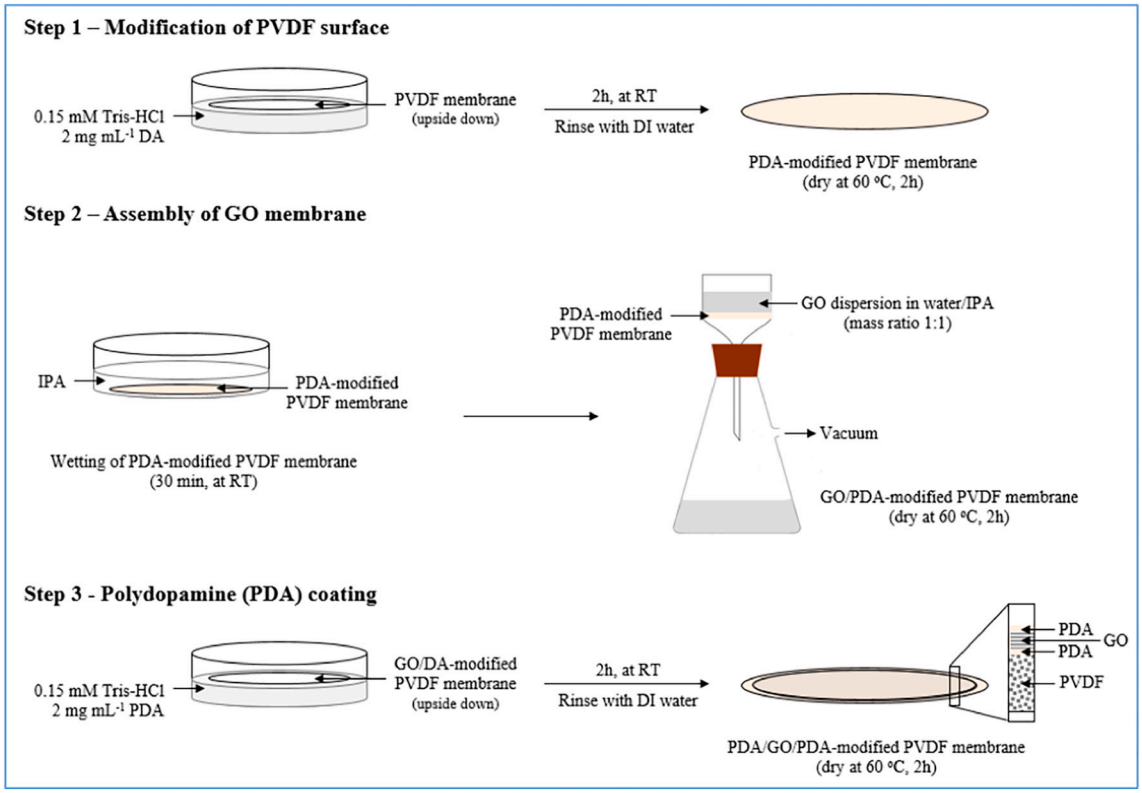

Fig. 2. Steps of membrane preparation: (1) modification of PVDF membranes with PDA, (2) formation of laminated GO membranes on PDA-modified PVDF membranes, and (c) PDA coating of laminated GO membrane. (GO: graphene oxide, DA: Dopamine hydrochloride, Tris-HCl: Tris(hydroxymethyl)aminomethane, PDA: polydopamine, PVDF: polyvinylidene fluoride, IPA: Isopropanol, RT: room temperature).

(2+2PDA) were prepared as a control. Table 1 shows the membrane codes according to their composition.

2.3. GO and membrane characterization

To study the lateral size of GO flakes, a Si/SiO_2 wafer was vertically submerged into an aqueous GO dispersion (0.05 mg mL^{-1}) and subsequently vertically withdrawn and let to dry horizontally. The flakes were imaged using a scanning electron microscope (SEM, Quanta FEG 250, USA) and the lateral flake size was measured using the open-source software ImageJ®.

Thermogravimetric analysis (TGA) of the GO powder was conducted using a TGA 550 thermogravimetric analyzer (TA Instruments, USA). This experiment was run under a nitrogen atmosphere with a gas flow of 10 mL min^{-1}, and a heating rate of 20 °C min^{-1}.

The Fourier transform infrared spectroscopy (FTIR) spectra of GO was acquired by using a VERTEX 70v FT-IR spectrometer (Bruker, USA) equipped with an attenuated total reflectance (ATR) accessory. The spectra were collected from 500 to 4000 cm^{-1}, at a scanning rate of 1 cm^{-1}.

Surface and cross-section morphologies of the membranes were investigated by SEM using also the Quanta FEG 250 microscope. To obtain cross-sectional samples, membranes were immersed in ethanol for a few seconds and freeze-dried using liquid nitrogen. A FEI Quanta 200 ESEM equipped with Energy dispersive X-ray spectroscopy (EDX) device was used to study the presence of NaCl on the permeate side of the membrane after MD experiments. All the samples were sputter-coated with a thin layer of palladium prior to imaging.

Capillary flow porometry (CFP) was employed to characterize the pore structure of the commercial PVDF membranes and was carried out using a Porolux 1000 porometer (Porolux, Belgium). Bubble point, mean flow pore (MFP) size, smallest pore size, and pore size distribution were determined by the wet/dry method. Firstly, PVDF samples (2.98 cm^2) were impregnated with the pore-filling liquid Porefl 125 (surface tension of 15.88 ± 0.03 mN/m, Porolux, Belgium). Nitrogen (N_2) gas was used to displace the liquid from the pores by increasing the gas pressure, giving the so-called wet curve (i.e. measured gas flow against the applied pressure). Following the wet curve, the N_2 flow against the applied pressure on the dry sample ("dry curve") was also measured. The pore size was calculated with Eq. (1):

$$P = \frac{4\gamma cos\theta}{D} \tag{1}$$

where P is the pressure required to displace the wetting liquid from the pore, D is the pore diameter, γ the surface tension of the wetting liquid and θ the contact angle of the wetting liquid. It is worth mentioning that this technique only takes into account open pores as the closed pores do not contribute to gas flow.

The surface roughness of all membranes was determined by atomic force microscopy (AFM), using a Fastscan microscope (Bruker, USA). The measurements were carried out at room temperature using tapping mode. The root mean square roughness (R_q) and the average roughness (R_a) were calculated using the Nanoscope analysis software version 1.5.

The surface hydrophobicity of the membranes before and after the induced-surfactant pore wetting was evaluated by measuring their water contact angles with a DSA100B Drop Shape Analyzer (KRUSS, Germany), using a sessile drop method with a 10 μL drop size of deionized water. The average values resulted from the water contact angles from at least 3 different locations on the membrane. Membranes were glued on a flat glass slide with double-sided tape.

Experimental liquid entry pressure (LEP) values of pristine PVDF and 40GO membranes (11.3 cm^2) were measured using a dead-end filtration cell (HP4750, Sterlitech, USA) filled with 200 mL of 35 g L^{-1} NaCl aqueous solution. Pressure was gradually applied on the feed side while allowing to stabilize after each increment. The LEP was recorded as the pressure at which the first drop of liquid permeate appears on the permeate side.

Leaching of GO was investigated by exposing pieces of the membranes (0.49 cm^2) to DI water (floating them with the coated side in contact with the water) under constant stirring. After an exposure time of 86 h, the amount of GO leached from the membrane was analyzed with UV–Visible spectroscopy (UV-2700 UV–Vis spectrophotometer, Shimadzu, UK). The absorption peak considered for GO appeared at 231 nm in the spectra, which corresponds to the $\pi \rightarrow \pi^*$ transitions for the C—C bonding [32]. Measurements were performed at room temperature using a quartz cuvette with a 1 cm optical path. Three different membrane structures were tested: GO on PVDF porous support (GO-PVDF), GO on 2 h PDA-treated PVDF porous support (GO-PDA-PVDF) and 40GO. All samples were prepared with the same GO density, and three samples of each were considered for the analyses.

2.4. Membrane distillation experiments

Pore wetting experiments were carried in an AGMD laboratory apparatus whose diagram is shown in Fig. 3. The feed solution was kept under constant stirring and constant temperature (75 °C) using a hot plate with a connected thermostat (MIL-C-17 ROHS, UK) and it was circulated at a constant rate of 1290 ± 55 mL min^{-1} using a 12 V water pump. The permeate was kept at 20 °C by a Julabo F12-ED chiller, which was circulated behind a stainless steel condenser plate at a rate of 600 ± 4 mL min^{-1}. The membrane cell had an air gap width of 3 mm and the effective membrane area was 9.1 cm^2. The permeate dripped out of the module by gravity and was collected in a measuring cylinder with a funnel placed below. All experiments started with 100 mL of DI water in the permeate tank in order to be able to record the online conductivity of the membrane permeate. To investigate the surfactant-induced pore wetting of the different membranes, Triton X-100 (150 ppm) was added to the aqueous feed solution. The online permeate conductivity and total flux were recorded using a digital conductivity meter (Go Direct Conductivity Probe, Instruments Direct Services Limited, UK), and a precision scale (HCB 6001, Adam Equipment, UK), respectively. At least three membranes of each composition were analyzed for surfactant-induced pore wetting.

The permeate flux (J, kg m^{-2} h^{-1}) was recorded and calculated using Eq. (2):

$$J = \frac{\Delta m_p}{A\Delta t} \tag{2}$$

where Δm_p is the change in the permeate mass tank (kg), A is the effective membrane area (m^2) and Δt is the sampling period.

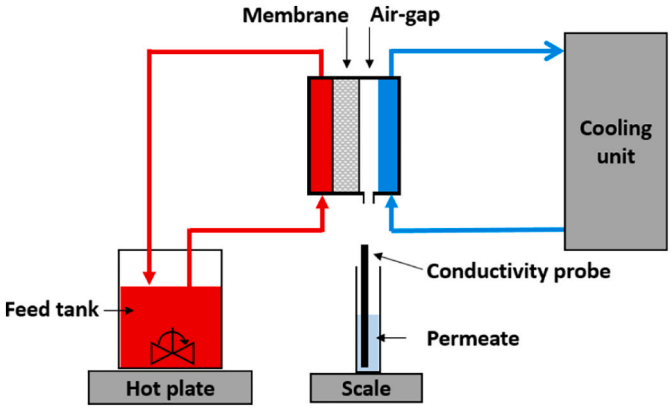

Fig. 3. Diagram of the AGMD unit used for conducting the experiments. Feed flow rate: 1290 ± 55 L min^{-1}, coolant water flow rate = 600 ± 4 mL min^{-1}. Effective membrane area: 9.1 cm^2. Feed and coolant temperatures of 75 °C and 20 °C, respectively.

The salt rejection (SR, %) is calculated using Eq. (3):

$$SR = \left(1 - \frac{C_p}{C_f}\right) \times 100\% \quad (3)$$

where C_p and C_f are the concentration of the permeate and feed, respectively.

3. Results and discussion

3.1. GO characterization

The lateral size distribution of the GO nanosheets was characterized through the image analysis of SEM images (Fig. S1a). According to the normal distribution curve-fitting that was used, the mean value of the lateral flakes size of GO is 3.5 ± 2.5 μm (Fig. S1b). Fig. S2a shows the TGA curve of GO. The first weight loss (~12 %) at temperature of up to 120 °C is due to the removal of physically adsorbed water molecules. The following weight loss is registered between 120 °C and 300 °C and corresponds to the decomposition of labile oxygen groups like epoxy and hydroxyl. The third weight loss occurring from 300 °C and 500 °C corresponds to the removal of more stable oxygen groups such as carbonyl. Above 500 °C, the pyrolysis of the carbon skeleton occurs [33]. The FTIR spectrum of GO (Fig. S2b) shows a broadband from 3000 and 3500 cm^{-1} associated with the O—H vibration, a band at 1725 cm^{-1} that corresponds to C═O vibrations, a band assigned to C═C stretching (1625 cm^{-1}), the C—O epoxide group stretching at 1223 and 1061 cm^{-1}, and a band associated to C-OH at 1376 cm^{-1} [34].

3.2. Membrane characterization

Figs. 4 and 5 show the surface and cross-sectional morphologies of PVDF, 2-PDA, 2 + 2PDA, 20GO, 40GO, and 60GO membranes, respectively. The SEM micrographs in Figs. 4a and 5a show the highly porous structure of the pristine PVDF membranes. Comparing Fig. 4b and c, an additional 2 h-PDA coating led to a more uniform but not complete coverage (2 + 2PDA, Fig. 4c) on the commercial PVDF membrane. It has been reported elsewhere that the amount of the PDA coating can be tuned by varying the number and reaction time of coating cycles; the longer the coating time and the higher the coating cycles, the greater is the amount of PDA deposited on the support [35], as shown for our control sample where 2 cycles of PDA coating have been carried out. Figs. 4d–f and 5d–f show the surface and cross-section of the membranes containing GO (20GO, 40GO, and 60GO), respectively. As expected, the increase in GO density led to a better membrane surface coverage and smoother surface, which was confirmed by AFM.

The surface roughness of all membranes was determined by AFM analysis, and their three-dimensional surface topography images are shown in Fig. 6. The surface roughness parameters (root mean square average roughness (R_q) and the average roughness (R_a)) are presented in Table 2. Pristine PVDF membranes showed the highest R_q and R_a values at 288 and 225 nm, respectively. The surface roughness of PDA-modified PVDF membranes decreased with an additional coating cycle; after the second 2-h PDA coating, the R_a value of 2PDA was reduced from 126 to 106 nm. Surface roughness consistently decreased upon the increase of GO density, reaching the lowest values of R_q (92 nm) and R_a (73 nm) for 60GO. These results are consistent with SEM images shown in Figs. 4 and 5.

The pore structure of pristine PVDF membranes was investigated through CFP. The analysis of the wet and dry curves (Fig. S3a) allowed the determination of the bubble point, MFP size, and smallest pore size, which were 570 ± 44, 484 ± 26, and 325 ± 14 nm, respectively. The pore size distribution of these membranes is shown in Fig. S3b.

Water contact angles of all membranes were measured before and after the surfactant-pore wetting tests and the results are presented in Table 2. As can be seen, the pristine PVDF membrane is hydrophobic with a water contact angle of 116° ± 3°. The water contact angle of PDA-modified PVDF membranes decreased due to the hydrophilic nature of PDA [36]; the water contact angles of 2PDA and 2 + 2PDA were 109 ± 4° and 69 ± 15°, respectively. As expected, the further addition of the laminated GO membrane and the second PDA layer maintained the hydrophilic nature of the membrane surface. In addition to PDA, GO exhibits hydrophilic properties due to the presence of oxygen-functional groups on its basal plane and edges of the nanosheets [37].

The experimental LEP values of pristine PVDF and 40GO membranes were also obtained and are displayed for these two membranes in Table 2. The pristine PVDF membrane showed a LEP value of 2.4 bar, while the 40GO membrane had a LEP of 4.6 bar. The increase upon coating, despite having a more hydrophilic surface, can be explained by

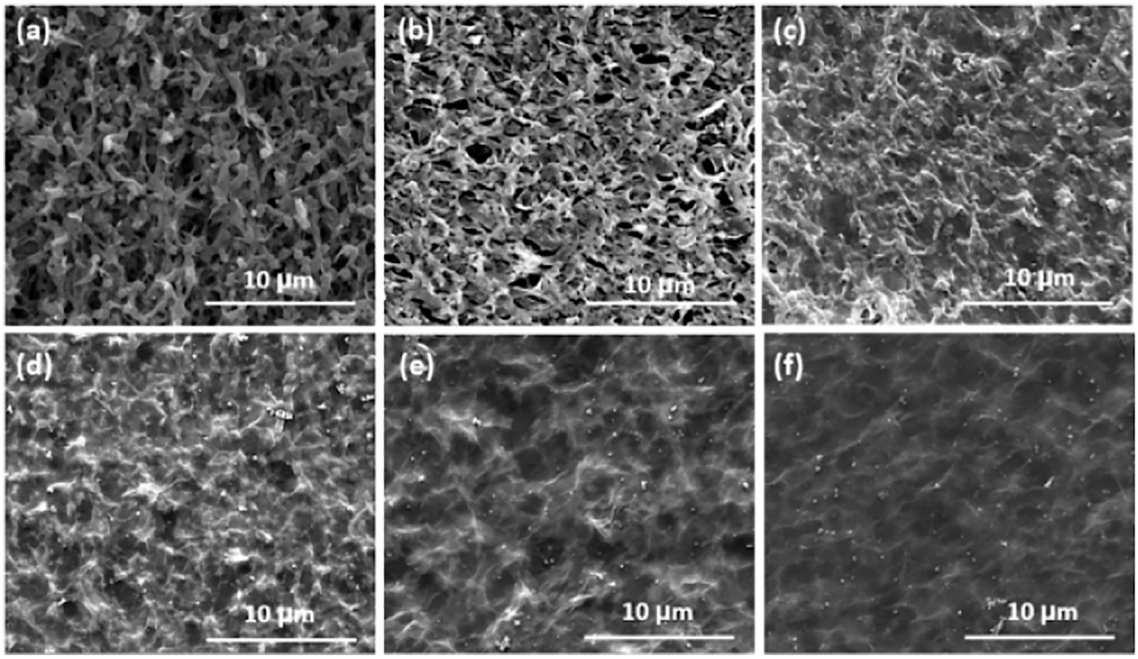

Fig. 4. SEM images of the surface of (a) PVDF, (b) 2PDA, (c) 2 + 2PDA, (d) 20GO, (e) 40GO and (f) 60GO.

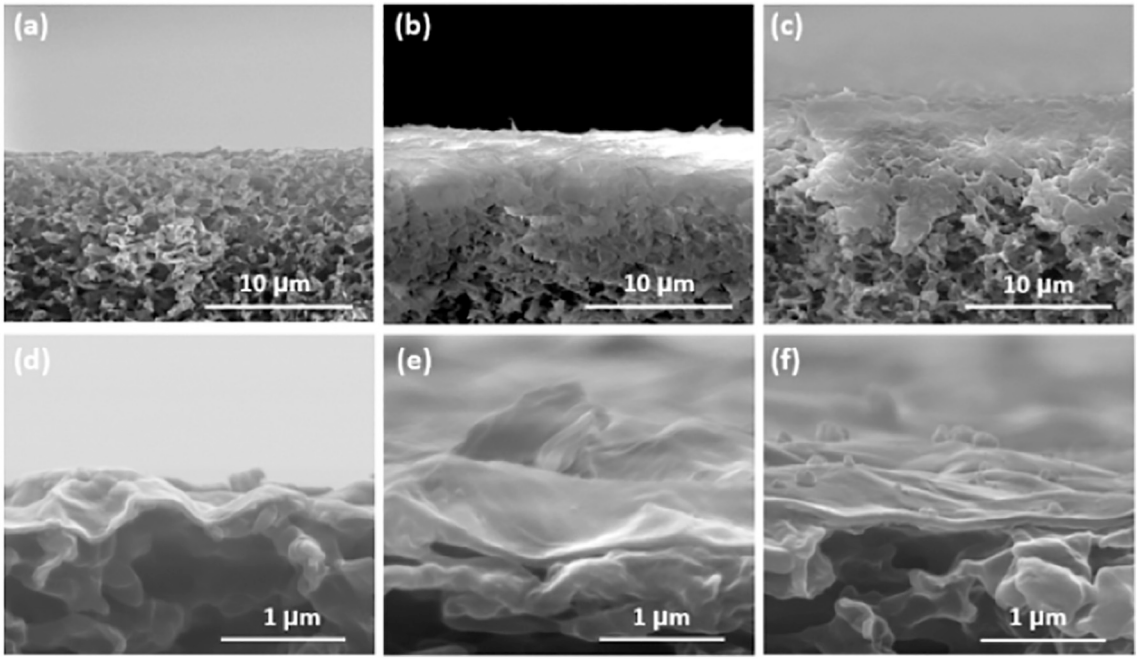

Fig. 5. SEM images of the cross section of (a) PVDF, (b) 2PDA, (c) 2 + 2PDA, (d) 20GO, (e) 40GO and (f) 60GO.

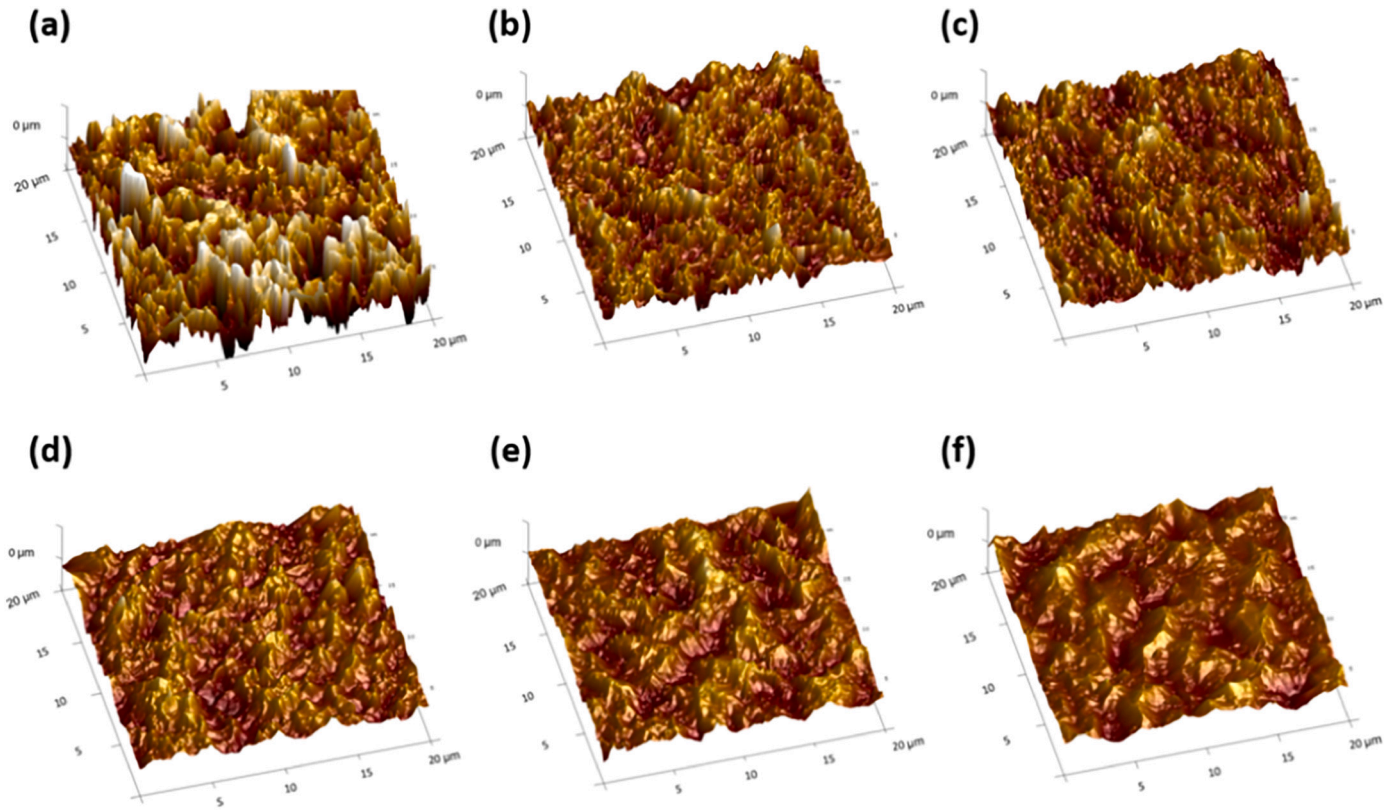

Fig. 6. 3D AFM images of (a) PVDF, (b) 2PDA, (c) 2 + 2PDA, (d) 20GO, (e) 40GO and (f) 60GO membranes.

the narrowed surface pore size of the GO membrane.

The stability of the GO coating in the 40GO membrane when exposed to water was evaluated through UV–Vis (calibration curve shown in Fig. S4a). The obtained spectra of the water after exposure of the GO coatings for a week are also shown in Fig. S4b. After 86 h, the percentages of GO detachment from the samples were found to be 30.5 %, 10.8 % and 9.6 % for GO-PVDF, GO-PDA-PVDF and 40GO, respectively. The decrease in GO detachment with the addition of an extra PDA layer on top of the GO coating is relatively low. However, it makes the membrane more resistant to handling and therefore the extra step should be justified for production of industrial membrane modules.

Table 2
Root mean square average roughness (R_q) and average roughness (R_a), liquid entry pressure, and water contact angle of membranes before and after the surfactant-induced pore wetting tests.

Membranes	R_q (nm)	R_a (nm)	Liquid entry pressure (bar)	Water contact angle (°)	
				Before pore wetting test	After pore wetting test
PVDF	288	225	2.4	116 ± 3	110 ± 4
2PDA	160	126		109 ± 4	–
2 + 2PDA	136	106		69 ± 15	47 ± 2
20GO	115	92		81 ± 4	17 ± 1
40GO	113	91	4.6	73 ± 2	16 ± 5
60GO	92	73		52 ± 2	44 ± 6

3.3. Membrane performance

The flux and NaCl rejection of all membranes were evaluated by using an aqueous feed solution containing 35 g L^{-1} NaCl. The feed and the permeate were kept at 75 and 20 °C, respectively. The average flux and NaCl rejection of all membranes are reported in Table S1 and plotted in Fig. 7 for easier visualization. The flux and rejection of the membranes were recorded after 2 h to allow for stabilization. Pristine PVDF membranes showed flux and NaCl rejection of 8.9 ± 1.2 kg m^{-2} h^{-1} and 99.98 ± 0.01 %, respectively. Although the highest average flux was obtained by the membrane 40GO (10.7 ± 1.2 kg m^{-2} h^{-1}), there are no significant changes in membrane performance upon the addition of laminated GO coatings, regardless of the thickness of the GO layer. Typically, the introduction of a new layer causes extra mass transfer resistance that leads to flux reduction [27]. However, in our study this is not observed, which could be explained by the unimpeded permeation of water vapor through the channels formed by the interlocked layered structure of micron-sized GO nanosheets [38]. Similar effects are reported in the literature when GO is used. Bhadra et al. [39] reported a significant increase in flux (up to 35 %) and mass transfer coefficient (up to 33 %) when drop-casting GO and PVDF (as a binder material) on commercial PVDF membranes. Besides the rapid transport of water vapor due to the nanocapillary effect, it is also suggested that the increase in flux is enhanced by the presence of polar functional groups such as epoxy, hydroxyl, and carboxyl on GO nanosheets that act as selective sorption sites for water vapor, and by the reduction of the temperature polarization. Following the same strategy as the above-mentioned study, Intrchom et al. [40] immobilized GO on the permeate side of commercial PTFE membranes and reported a flux increment of 15 % compared to pristine membranes. They suggested that this enhancement in membrane performance was due to the rapid removal of the permeate water vapor from the membrane-permeate stream interface causing an enhancement of the mass transfer coefficient. In our work, the additional mass transfer resistance of the fabricated membranes could be offset by the increase in polar groups of GO which can act as absorption sites and increased heat transfer resistance from the insulating PDA layer that leads to lower heat losses. Although the hydrophilicity of the GO membranes was higher than the pristine PVDF, the results suggest that this increase in hydrophilicity is counter-acted by the sharp decrease in surface pore size as seen in SEM images in Fig. 4. The overall resulting impact on the separation mechanics is an increase in LEP and thus an increase in pore-wetting resistance. This finding is supported by McGaughey et al. [41] who reported that reducing the pore size can be more effective than increasing the hydrophobicity when developing wetting-resistant membranes.

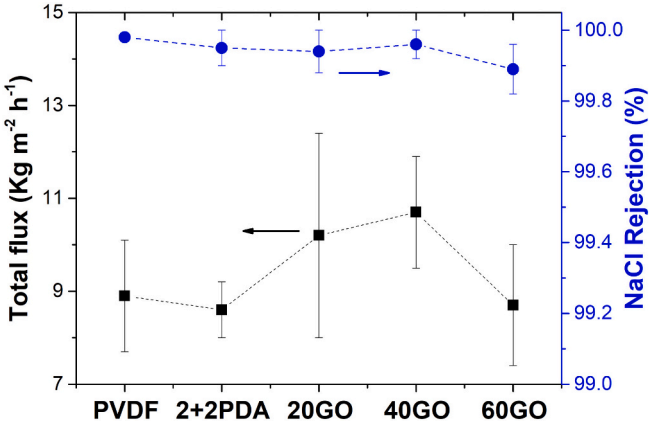

Fig. 7. Average total flux and NaCl rejection of the prepared membranes. Aqueous feed solution: 35 g L^{-1} NaCl. Feed and permeate temperatures of 75 and 20 °C, respectively. Average values of the total flux and NaCl rejection resulted from at least three samples of the same membrane type. ■: membrane flux (kg m^{-2} h^{-1}), and ●: salt rejection. Error bars stand for the standard deviation of the set of values gathered for at least three samples with the same composition.

The surfactant-induced pore wetting of all membranes was evaluated by adding Triton X-100 (150 ppm) into the saline feed solutions (35 g L^{-1} NaCl aqueous solution) once the steady state had been reached. The total flux and permeate conductivity were evaluated for at least three samples with the same composition. To compare the response of the membrane upon the addition of the surfactant, the addition of Triton X-100 was aligned to 30 min for all membranes.

Fig. 8a shows the response of commercial PVDF membranes upon the addition of the surfactant. As can be seen, the addition of surfactant led to a total failure of the MD performance of commercial PVDF membranes, which was demonstrated by a sharp rising of the permeate conductivity, accompanied by an increase in the total permeate flux. Similar studies showing identical pore wetting effects have been reported in the literature [19,42,43]. Surfactants lower the surface tension of the feed, causing a reduction in the liquid entry pressure (LEP) and consequently a greater propensity for membrane wetting. It is stated that the membrane wetting rate is also dependent on the hydrophilic-lipophilic balance (HLB), critical micelle concentration (CMC) values of the surfactant [42], and the excess concentration of the surface surfactant on membrane pore surface [44].

The purpose of depositing a second PDA layer was to maintain the integrity and prevent delamination of the GO laminated membranes during mounting and dismounting the membranes and throughout the MD tests. As a control, 2 + 2PDA membranes were also tested and the results are shown in Fig. 8b. Although the doubled 2 h-PDA coating on pristine PVDF membranes showed a delay of the membrane pore wetting, it did not prevent the complete failure of the MD performance upon the presence of surfactant in the feed solution. As seen in the SEM image of the membrane surface in Fig. 4c, the PDA coating did not cover the entire surface of PVDF membranes, so the surfactant molecules were able to reach the PVDF membrane causing the membrane pore wetting.

Fig. 9a–c shows the performance of 20GO, 40GO, and 60GO membranes when subjected to a saline feed solution containing surfactant. Each experiment was repeated at least three times. According to the data obtained, the permeate conductivity reached maximum values of 17.3, 28.4, and 17.4 μS cm^{-1} for 20GO, 40GO, and 60GO, respectively, after 150 min after the addition of the surfactant. The low permeate conductivity is an indication that the GO laminated layer significantly enhanced the surfactant-induced pore wetting resistance of pristine PVDF membranes. As suggested by Qiu et al. [27], the GO coating acts as a protective skin layer that prevents the surfactant molecules to reach the hydrophobic PVDF membrane which helps the minimization of wetting effects caused by the presence of the surfactant in the feed solution. The same study also showed that the charge of the surfactant might also affect the role of the GO in the membrane.

In this context, Seo et al. [28] demonstrated that the deposition of a few-layer graphene layer onto a commercial PFTE membrane improved not only the flux by approximately 20 % when real seawater was used as a feed, but also the stability of the membrane performance when using a

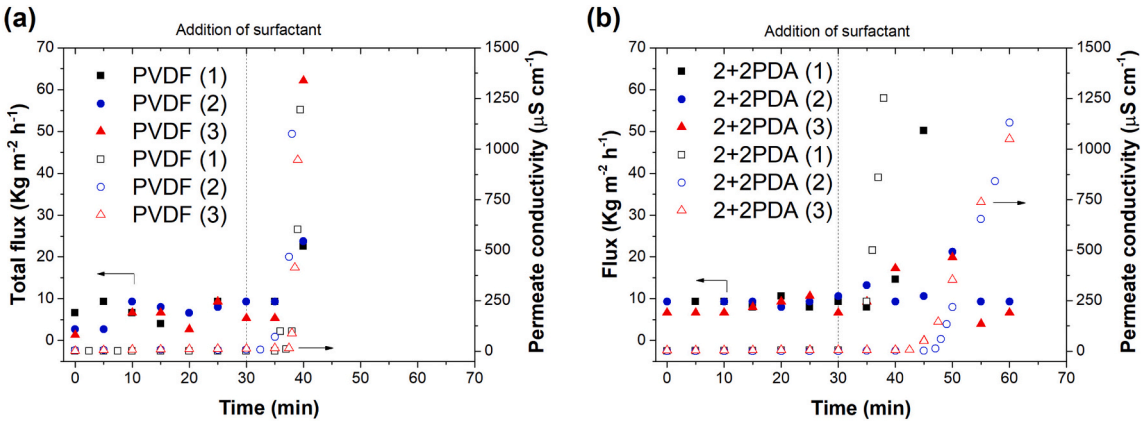

Fig. 8. (a) Performance of commercial PVDF, and (b) 2 + 2PDA membranes upon the addition of Triton X-100 (150 ppm). Three samples were tested and each set of symbols represents one PVDF membrane. Full and empty symbols represent the membrane flux and the permeate conductivity, respectively. Numbers in between brackets in (1), (2), and (3) represent the sample number.

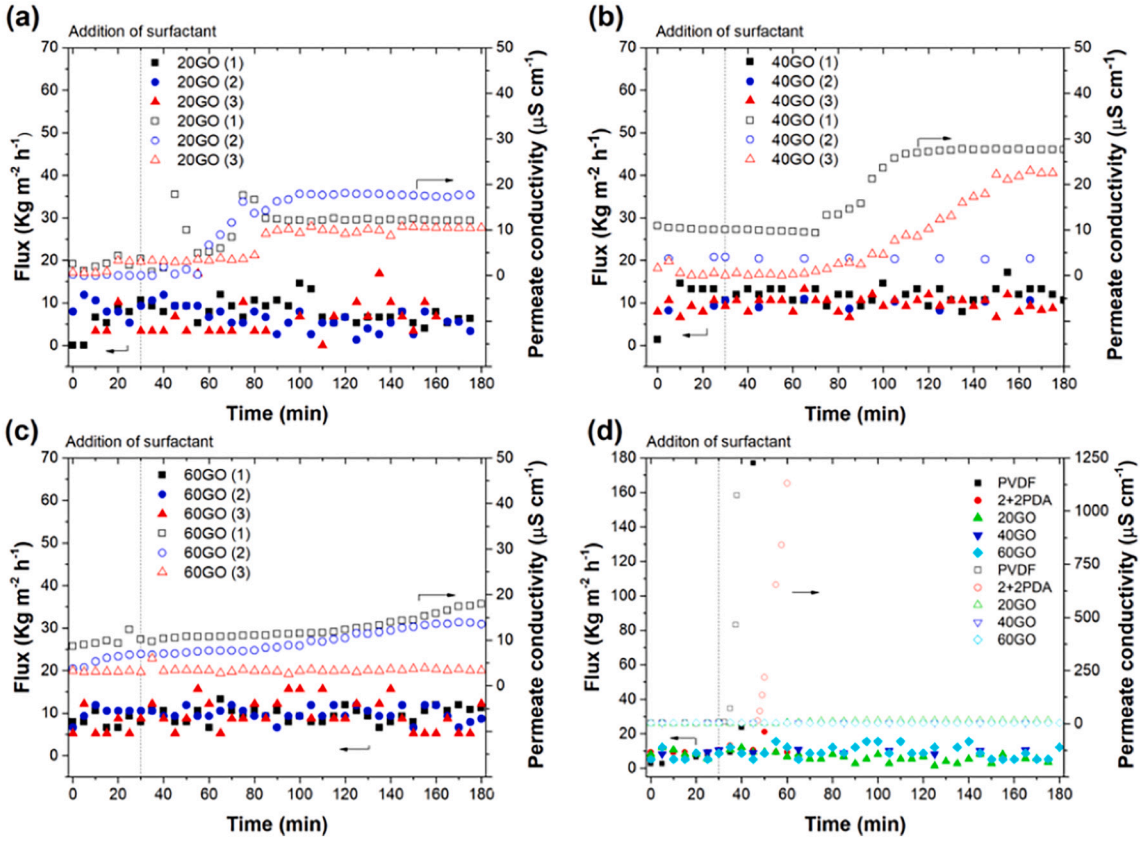

Fig. 9. Total flux and permeate conductivity of (a) 20GO, (b) 40GO, and (c) 60GO upon the addition of surfactant (Triton X-100, 150 ppm), and (d) a comparison of membrane performance. Numbers in between brackets in (a), (b), and (c) represent the sample number.

feed containing a surfactant (sodium dodecyl sulphate (SDS)). This enhancement in membrane performance is justified by: (i) a reduction of attached fouling molecules on the membrane surface reducing the pore-blocking effect, (ii) the weak physisorption between the graphene and SDS that can be easily overcome by the feed flow rate, and (iii) facilitated water vapor transport across nanochannels aided by the mismatched and overlapping of graphene domains.

The long-term performance stability of the membrane 40GO was evaluated for 90 h, and the results are shown in Fig. 10. The membrane rejection remains above 99.999 % for 70 h, where it decreases to >98 %. A sharp increase in flux occurs after ~60 h after gradually decreasing over the first 50 h. The exact reason behind the reduction of the flux is not very clear at this stage, however, one reason could be the adsorption of the surfactant onto the membrane surface. The increase in flux after 60 h could be related to partial detachment of the GO coating, as confirmed by the leaching experiments (9.6 % detachment after 86 h for GO40). Also, the reason for the fluctuation in the flux is not well understood but could be due to the operational procedure, as most hikes in water flux occur when fresh water is added to the feed tank to restabilize initial salt and surfactant concentrations. However, the most promising outcome of the long term experiment is that unlike with pristine PVDF, the adsorption of the surfactant onto the GO-PDA-coated membranes

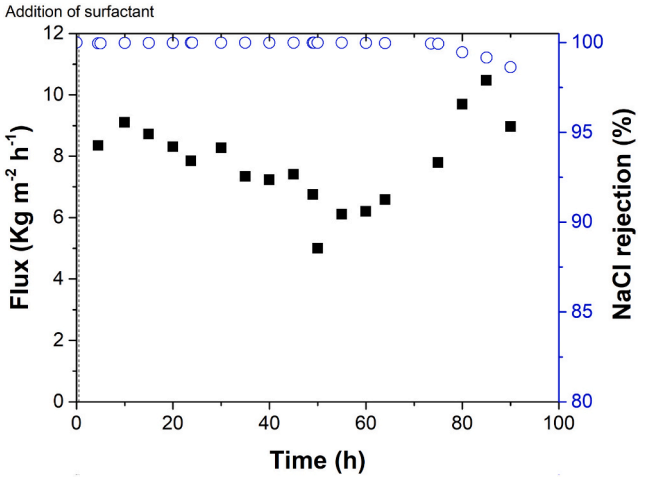

Fig. 10. Long-term performance of the PDA-GO-PDA-coated membrane 40GO upon the addition of the surfactant (Triton X-100, 150 ppm). ■: membrane flux (kg m^{-2} h^{-1}), and ○: salt rejection (%).

does not lead to immediate and catastrophic pore wetting. The salt rejection stays high over prolonged times due to the increased LEP and the relatively high stability of the coating.

It is worth noting that a study by González et al. [45] on the characterization of surfactants in textile wastewater reported that the most prevalent surfactants were found in concentrations ranging from 0.93 to 5.68 ppm and 0.06 to 4.30 ppm for nonylphenol ethoxylate (NPEO) and NPEO-SO_4 respectively. The concentrations investigated in this study are an order of magnitude higher than this, and they are also higher than those previously investigated for MD [13,46]. Thus, it is expected that these membranes can have longer-term stability, and higher flux when lower surfactant concentration are use, and thus could be used for a variety of industrial processes. The membranes should be also mounted into modules and tested at larger-scale to study their performance.

SEM and EDX analyses were performed to evaluate the presence of NaCl on the permeate side of a 40GO membrane after the MD 5 h-experiment (Fig. S5). Some areas of the membrane back surface showed some evidence of NaCl. Upon performing EDX analysis on the area highlighted in Fig. S6 (shown by the red rectangle), it was observed that both Na and Cl elements as well as C and F from the PVDF were present. However, it should be noted that the majority of the membrane back surface did not show presence of NaCl (e.g. Fig. S7). These results are in agreement with the very high salt rejection that is achieved in the tested interval.

4. Conclusions

The development of MD membranes to successfully desalinate saline water with a complex composition is still a challenge. While recent studies have shown promising results, pore wetting is still a phenomenon that is hindering the wider use of this membrane separation process.

In this study, surfactant-induced pore wetting-resistant GO-based membranes were successfully prepared. A tri-layer structure consisting of a GO laminated membrane in between two PDA coatings, and deposited on commercial PVDF showed to be an effective method to not only prepare stable GO laminated membranes which did not detach, but also to prevent the pore-wetting effects caused by the presence of a non-ionic surfactant (Triton X-100) in the saline feed solution. This was achieved without compromising the membrane flux in the absence of surfactants, even though three extra layers were added to the PVDF membrane. The long-term stability test also showed that the membrane rejection remained above 99.9 % over 70 h, but this was accompanied by a reduction of flux over time, that could be less severe when working at lower surfactant concentration.

The results suggest that through the addition of a tri-layer coating on top of a commercial membrane, MD can be used to produce potable water from feedwaters containing surfactants. This could allow a more widespread commercialisation of MD within wastewater treatment. For future work, the flux fluctuations and preparation of membranes with longer-term stability (i.e. with complete prevention of GO leaching) should be investigated at other feed compositions with a variety of surfactants, including real-world samples, and in addition, adopting a soft cleaning regime where necessary. This will be used to have a better understanding of how the membranes would perform industrially.

CRediT authorship contribution statement

Monica Alberto: Conceptualization, Investigation, Methodology, Formal analysis, Visualization, Writing - Original Draft.

Clara Skuse: Investigation, methodology, Writing - Review & Editing.

Marzieh Tamaddondar: Methodology.

Patricia Gorgojo: Conceptualization, Supervision, Project administration, Funding acquisition, Writing - Review & Editing.

Declaration of competing interest

All authors have no actual or potential conflict of interest including any financial, personal or other relationships with other people or organizations within three years of beginning the submitted work that could inappropriately influence, or be perceived to influence, their work.

Acknowledgments

The authors acknowledge the Engineering and Physical Sciences Research Council (EPSRC) grant EP/S032258/1 for supporting this work. Clara Skuse would like to acknowledge the EPSRC for funding this work through the NOWNANO CDT. Patricia Gorgojo is grateful to the Spanish Ministerio de Economía y Competitividad and the European Social Fund for her Ramón y Cajal Fellowship (RYC2019-027060-I/AEI/10.13039/501100011033).

Appendix A. Supplementary data

Supplementary data to this article can be found online at https://doi.org/10.1016/j.desal.2022.115898.

References

[1] P. Burek, et al., Water Futures And Solution -Fast Track Initiative (Final Report), 2016.
[2] M. Gryta, Influence of polypropylene membrane surface porosity on the performance of membrane distillation process, J. Membr. Sci. 287 (1) (2007) 67–78.
[3] H. Kim, et al., Experimental and theoretical investigation of a high performance PTFE membrane for vacuum-membrane distillation, J. Membr. Sci. 617 (2021), 118524.
[4] M. Tian, et al., One-step fabrication of isotropic poly(vinylidene fluoride) membranes for direct contact membrane distillation (DCMD), Desalination 477 (2020), 114265.
[5] S. Leaper, et al., Flux-enhanced PVDF mixed matrix membranes incorporating APTS-functionalized graphene oxide for membrane distillation, J. Membr. Sci. 554 (2018) 309–323.
[6] Y. Chen, et al., Probing pore wetting in membrane distillation using impedance: early detection and mechanism of surfactant-induced wetting, Environ.Sci. Technol.Lett. 4 (11) (2017) 505–510.
[7] V. Belessiotis, S. Kalogirou, E. Delyannis, Chapter four - membrane distillation, in: V. Belessiotis, S. Kalogirou, E. Delyannis (Eds.), Thermal Solar Desalination, Academic Press, 2016, pp. 191–251.
[8] C. Skuse, et al., Can emerging membrane-based desalination technologies replace reverse osmosis? Desalination 500 (2021), 114844.
[9] A.A. Kiss, O.M. Kattan Readi, An industrial perspective on membrane distillation processes, J. Chem. Technol. Biotechnol. 93 (8) (2018) 2047–2055.
[10] E. Guillen-Burrieza, et al., Understanding wetting phenomena in membrane distillation and how operational parameters can affect it, J. Membr. Sci. 515 (2016) 163–174.

[11] M.R. Choudhury, et al., Fouling and wetting in the membrane distillation driven wastewater reclamation process – a review, Adv. Colloid Interf. Sci. 269 (2019) 370–399.
[12] M. Zhu, Y. Mao, Large-pore-size membranes tuned by chemically vapor deposited nanocoatings for rapid and controlled desalination, RSC Adv. 10 (66) (2020) 40562–40568.
[13] Z. Wang, et al., Mechanism of pore wetting in membrane distillation with alcohol vs. surfactant, J. Membr. Sci. 559 (2018) 183–195.
[14] Z. Wang, S. Lin, Membrane fouling and wetting in membrane distillation and their mitigation by novel membranes with special wettability, Water Res. 112 (2017) 38–47.
[15] A. Abdel-Karim, et al., Membrane cleaning and pretreatments in membrane distillation – a review, Chem. Eng. J. 422 (2021), 129696.
[16] S. Lin, et al., Omniphobic membrane for robust membrane distillation, Environ.Sci. Technol.Lett. 1 (11) (2014) 443–447.
[17] C. Boo, J. Lee, M. Elimelech, Omniphobic polyvinylidene fluoride (PVDF) membrane for desalination of shale gas produced water by membrane distillation, Environ.Sci.Technol. 50 (22) (2016) 12275–12282.
[18] Y. Chul Woo, et al., CF4 plasma-modified omniphobic electrospun nanofiber membrane for produced water brine treatment by membrane distillation, J. Membr. Sci. 529 (2017) 234–242.
[19] W. Qing, et al., Omniphobic PVDF nanofibrous membrane for superior anti-wetting performance in direct contact membrane distillation, J. Membr. Sci. 608 (2020), 118226.
[20] T. Chen, et al., Development of robust and superamphiphobic membranes using reduced graphene oxide (rGO)/PVDF-HFP nanocomposite mats for membrane distillation, Environ.Sci.Nano 8 (10) (2021) 2883–2893.
[21] P. Peng, A.G. Fane, X. Li, Desalination by membrane distillation adopting a hydrophilic membrane, Desalination 173 (1) (2005) 45–54.
[22] L.N. Nthunya, et al., Fouling-resistant PVDF nanofibre membranes for the desalination of brackish water in membrane distillation, Sep. Purif. Technol. 228 (2019), 115793.
[23] M. Rezaei, et al., Wetting prevention in membrane distillation through superhydrophobicity and recharging an air layer on the membrane surface, J. Membr. Sci. 530 (2017) 42–52.
[24] D.M. Warsinger, et al., Combining air recharging and membrane superhydrophobicity for fouling prevention in membrane distillation, J. Membr. Sci. 505 (2016) 241–252.
[25] J. Zahirifar, et al., Fabrication of a novel octadecylamine functionalized graphene oxide/PVDF dual-layer flat sheet membrane for desalination via air gap membrane distillation, Desalination 428 (2018) 227–239.
[26] S. Leaper, et al., POSS-functionalized graphene oxide/PVDF electrospun membranes for complete arsenic removal using membrane distillation, ACS Appl. Polym.Mater. 3 (4) (2021) 1854–1865.
[27] H. Qiu, et al., Pore channel surface modification for enhancing anti-fouling membrane distillation, Appl. Surf. Sci. 443 (2018) 217–226.
[28] D.H. Seo, et al., Anti-fouling graphene-based membranes for effective water desalination, Nat. Commun. 9 (1) (2018) 683.
[29] T. Huang, et al., Polydopamine coated graphene oxide aerogels and their ultrahigh adsorption ability, Diam. Relat. Mater. 86 (2018) 117–127.
[30] G. Zin, et al., Modification of hydrophobic commercial PVDF microfiltration membranes into superhydrophilic membranes by the mussel-inspired method with dopamine and polyethyleneimine, Sep. Purif. Technol. 212 (2019) 641–649.
[31] K. Xu, et al., Synthesis of highly stable graphene oxide membranes on polydopamine functionalized supports for seawater desalination, Chem. Eng. Sci. 146 (2016) 159–165.
[32] J.I. Paredes, et al., Graphene oxide dispersions in organic solvents, Langmuir 24 (19) (2008) 10560–10564.
[33] T. Ko, et al., Sulfonated poly(arylene ether sulfone) composite membranes having poly(2,5-benzimidazole)-grafted graphene oxide for fuel cell applications, J. Mater. Chem. A 3 (41) (2015) 20595–20606.
[34] J. Pei, et al., Fabrication of reduced graphene oxide membranes for highly efficient water desalination, RSC Adv. 6 (104) (2016) 101948–101952.
[35] X. Wu, et al., Localized heating with a photothermal polydopamine coating facilitates a novel membrane distillation process, J. Mater. Chem. A 6 (39) (2018) 18799–18807.
[36] Y. Liu, K. Ai, L. Lu, Polydopamine and its derivative materials: synthesis and promising applications in energy, environmental, and biomedical fields, Chem. Rev. 114 (9) (2014) 5057–5115.
[37] S. Pei, H.-M. Cheng, The reduction of graphene oxide, Carbon 50 (9) (2012) 3210–3228.
[38] R.R. Nair, et al., Unimpeded permeation of water through helium-leak–tight graphene-based membranes, Science 335 (6067) (2012) 442.
[39] M. Bhadra, S. Roy, S. Mitra, Desalination across a graphene oxide membrane via direct contact membrane distillation, Desalination 378 (2016) 37–43.
[40] W. Intrchom, et al., Immobilization of graphene oxide on the permeate side of a membrane distillation membrane to enhance flux, Membranes 8 (3) (2018).
[41] A.L. McGaughey, et al., Hydrophobicity versus pore size: polymer coatings to improve membrane wetting resistance for membrane distillation, ACS Appl.Polym. Mater. 2 (3) (2020) 1256–1267.
[42] N.G.P. Chew, et al., Surfactant effects on water recovery from produced water via direct-contact membrane distillation, J. Membr. Sci. 528 (2017) 126–134.
[43] D. Hou, et al., Biomimetic superhydrophobic membrane for membrane distillation with robust wetting and fouling resistance, J. Membr. Sci. 599 (2020), 117708.
[44] Z. Wang, et al., Significance of surface excess concentration in the kinetics of surfactant-induced pore wetting in membrane distillation, Desalination 450 (2019) 46–53.
[45] S. González, et al., Characterization and quantitative analysis of surfactants in textile wastewater by liquid chromatography/quadrupole-time-of-flight mass spectrometry, Rapid Commun. Mass Spectrom. 22 (10) (2008) 1445–1454.
[46] D. Hou, et al., Effect and mechanism of an anionic surfactant on membrane performance during direct contact membrane distillation, J. Membr. Sci. 595 (2020), 117495.